A Platinum Open Access Journal for Organic Chemistry

Paper

Free to Authors and Readers | DOAJ Seal | *Arkivoc* **2025** (5) 202512385

Synthetic strategies and structure-activity relationships of 2-chloro-tetrahydrocarbazolones: privileged organic scaffolds targeting polyketide synthase 13 for antitubercular activity

Priyanka Sanjay Waghmare[a], Anuruddha Rajaram Chabukswar*[a], Samidha Sameer Bag[a], Pratik Sanjay Manka[a], and Swati Changdeo Jagdale[a]

[a] *Department of Pharmaceutical Sciences, School of Health Sciences and Technology, Dr. Vishwanath Karad MIT-World Peace University, Kothrud, Pune, Maharashtra, India- 411038*
Email: anuruddha.chabukswar@mitwpu.edu.in

Received 04-04-2025 **Accepted** 06-26-2025 **Published on line** 07-16-2025

Abstract

This study explores the potential of tetrahydrocarbazole derivatives as anti-tubercular agents through in silico and *in vitro* evaluations. A three-step synthetic pathway was developed to access novel 2-chloro-2,3,4,9-tetrahydro-1*H*-carbazol-1-one derivatives, utilizing regioselective oxidation and electrophilic chlorination. Structures were confirmed via IR, NMR, and HRMS, reinforcing the importance of synthetic organic chemistry in medicinal scaffold development. Among the synthesized compounds, **12** exhibited the most potent activity, outperforming standard drugs Isoniazid and Rifampicin.

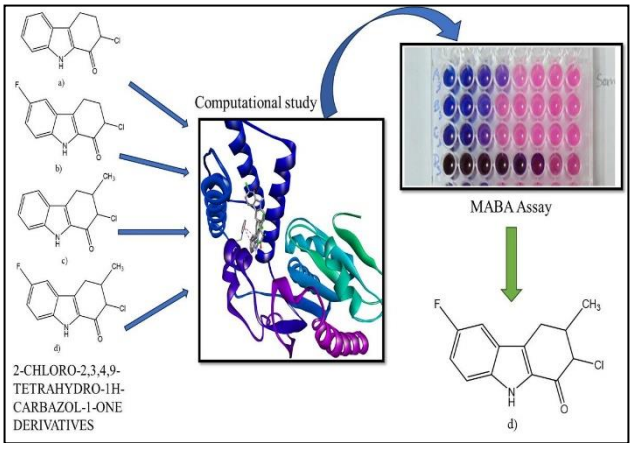

Keywords: 2-Chloro-2,3,4,9-tetrahydro-1*H*-carbazol-1-one; organic synthesis; heterocyclic chemistry; docking; spectroscopy; MABA assay

Introduction

Despite two decades of intensified research aimed at understanding and treating tuberculosis (TB), significant biological uncertainties persist, hindering progress. TB remains the second-leading infectious killer worldwide, following COVID-19. According to the WHO's 2022 report (updated on November 7, 2023), an estimated 10.6 million people contracted TB globally, including 5.8 million men, 3.5 million women, and 1.3 million children. TB affects all countries and age groups. In high-burden countries like India, vital registration systems often lack sufficient coverage to provide accurate mortality estimates. Consequently, TB incidence and mortality rates are typically estimated indirectly using available data [1]. Treatment failure has become increasingly prevalent due to drug resistance, necessitating the use of more toxic and expensive medications. Bedaquiline, Pretomanid, and Linezolid (Figure 1) are currently the only three drugs approved as part of a six-month regimen for treating MDR TB, caused by resistance to Isoniazid (INH) and Rifampicin—and XDR TB, characterized by resistance to Rifampicin, INH, quinolones, and aminoglycosides. These medications feature two novel mechanisms of action.[2] Given the prolonged and costly nature of these treatments, there is an urgent need for shorter, more effective regimens, either through the development of new drugs or by optimizing drug combinations to enhance efficacy. [3] The current treatment outcomes remain suboptimal, primarily due to extensive genetic mutations in Mycobacterium tuberculosis (Mtb) and widespread drug resistance [4,5]. This has driven an intensive search for novel, potent anti-TB agents. Fully understanding the mechanisms of action of established anti-TB drugs is critical, as drug development is both costly and time-intensive. Exploring alternatives with improved pharmacokinetic properties and reduced toxicity represents a promising avenue for creating effective new therapies.

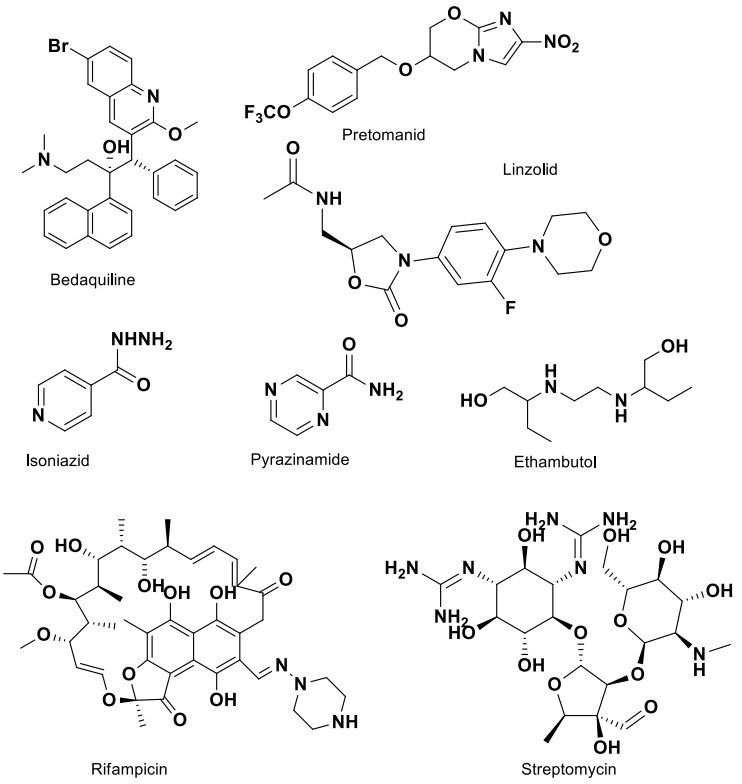

Figure 1. Chemical structure of drug approved in 2019 for the treatment of MDR TB (Bedaquiline, Pretomanid and Linezolid) and First line drugs (INH, Pyrazinamide, Rifampicin, Streptomycin, Ethambutol).

The escalating problem of drug resistance necessitates the exploration of new chemotypes with distinct mechanisms of action. Natural product-inspired heterocycles remain a valuable starting point in this regard. Among these tetrahydrocarbazole is a prominent tricyclic scaffold known for its diverse biological activities like anticancer [6], antibiotic [7], antidepression [8], analgesic [9], antiviral [10,11] etc. Because of its special balance of aliphatic and aromatic properties, tetrahydrocarbazole is a useful building block for the synthesis of many different kinds of chemicals [12]. From an organic chemistry standpoint, tetrahydrocarbazole derivatives provide a versatile template for functionalization. The electron-rich nitrogen-containing core allows for regioselective substitution, facilitating the synthesis of diverse analogs with tunable biological properties. In particular, the installation of electron-withdrawing groups such as halogens can improve membrane permeability, metabolic stability, and binding affinity to protein targets. The presence of a ketone functionality in the 1-position of the scaffold enhances hydrogen bonding potential, which can be leveraged to improve target specificity. Moreover, synthetic methodologies enabling such modifications—oxidation, halogenation, and ring fusion—are well-established in heterocyclic chemistry, rendering this class of compounds highly attractive for lead development.

The potential of tetrahydrocarbazole derivatives as anti-TB agents has remained underexplored despite their favorable physicochemical properties and synthetic accessibility. Predictive studies suggest that these derivatives could offer shorter, safer, and more effective treatment options for TB. Polyketide synthase 13 (Pks13) is a critical enzyme involved in the synthesis of mycolic acid, a key component of the Mtb cell wall [13]. Inhibiting Pks13 disrupts mycolic acid production, impairing the survival and replication of Mtb. Consequently, Pks13 has emerged as a compelling target for anti-TB drug development[14,15]. Several recent studies have validated Pks13 as a druggable enzyme using both biochemical and structural approaches. Therefore, identifying small molecules capable of binding to and inhibiting Pks13 is a strategic direction in TB therapeutics. In this context, tetrahydrocarbazole-based molecules offer a promising molecular architecture that could be exploited to target this essential enzyme.

The present study was designed to synthesize and evaluate a novel series of 2-chloro-2,3,4,9-tetrahydro-1H-carbazol-1-one derivatives with potential anti-TB activity, specifically aimed at inhibiting Pks13. A concise three-step synthetic route was developed, involving acid-catalyzed cyclization, periodic acid oxidation, and copper(II)-mediated chlorination. The derivatives were structurally characterized by infrared spectroscopy (IR), proton nuclear magnetic resonance (^{1}H NMR), and high-resolution mass spectrometry (HRMS). In parallel, computational studies, have revolutionized drug design, enabling the generation and optimization of active compounds for combating global TB drug resistance [16]. A molecular docking study was conducted on the crystal structure of Mtb Pks13 (PDB ID: 5V3Y) to assess the binding affinity and interactions between the ligand and receptor [17]. Additionally, an ADMET (absorption, distribution, metabolism, elimination, and toxicity) analysis is essential to evaluate drug-like properties [18]. Structure-based drug design facilitates the creation of molecules that effectively block the target protein while exhibiting favourable physiological properties. In developing anti-TB agents, in vitro studies are crucial. MICs are used to measure antimycobacterial activity, with standard anti-TB drugs INH, Rifampicin, Streptomycin, Pyrazinamide, and Ethambutol (Figure 1) serving as reference points [19].

In summary, this work integrates synthetic organic chemistry, computational modeling, and biological evaluation to explore a new class of heterocyclic compounds as anti-TB agents. The focus on tetrahydrocarbazole derivatives underscores the significance of heterocyclic scaffolds in the rational design of bioactive molecules. The results offer valuable insights into structure–activity relationships and lay the groundwork for further optimization of this scaffold for TB therapy.

Results and Discussion

2.1 Chemistry and Characterisation

Scheme 1 presented the synthetic method. The oxidation of tetrahydrocarbazole (**1**) to substituted oxo-tetrahydrocarbazole (**5**) using periodic acid involves the selective introduction of a ketone group. Periodic acid (HIO_4), pre-cooled to 0°C, acts as a strong oxidizing agent and facilitates the oxidation of the methylene group adjacent to the nitrogen atom in **1**. Initially, periodic acid abstracts a hydride ion (H^-) from the methylene group, forming an iminium ion intermediate. Water, present in the reaction mixture, then attacks the iminium ion, leading to hydrolysis and the formation of a carbonyl group (-C=O) at the site of oxidation. This transformation is highly selective, ensuring the formation of the substituted oxo-tetrahydrocarbazole (**5**) without over-oxidizing other parts of the molecule. The reaction is carefully controlled by maintaining a low temperature (0°C) during the initial phase to avoid side reactions, followed by stirring at room temperature for 1–1.5 hours to complete the oxidation process. This results in the efficient and clean formation of the desired product with good yield. In the last step, $CuCl_2$ dissociates in DMSO, generating Cu^{2+} and Cl^- ions. The Cu^{2+} acts as a Lewis acid, coordinating with the oxygen atom of the ketone group in **5**, thereby increasing the electrophilicity of the carbonyl carbon. This activation facilitates a nucleophilic attack by the chloride ion (Cl^-) on the carbonyl carbon, forming a tetrahedral intermediate. Subsequent elimination of a hydroxyl group leads to the formation of the final product (**9**), which contains a chlorine atom at the α-position relative to the ketone group. The reaction mixture is then cooled in an ice bath, leading to the precipitation of the product.

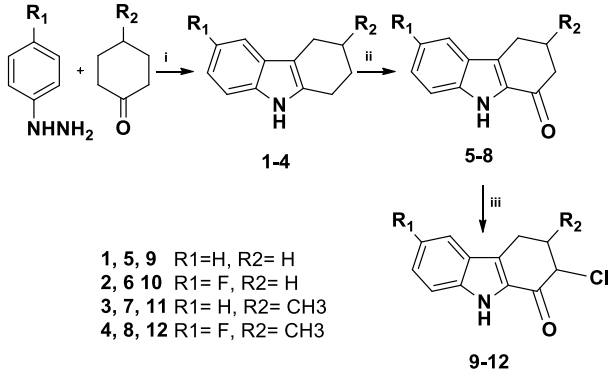

Scheme 1. Synthesis of substituted 2-chloro-2,3,4,9-tetrahydro-1H-carbazol-1-one (**9-12**): Reagents and condition (i) Glacial acetic acid, 3hrs reflux, (ii) periodic acid, methanol, water, stirred at 0°C for 1hr. then 1 -1.5 hrs. at room temperature (iii) Copper chloride, Dimethyl sulphoxide, stirred at 120°C, 15 min.

It is important to evaluate the chemical stability, reactivity, and biological activity of the tetrahydrocarbazole core upon substitution with both electron-withdrawing and electron-donating functional groups at specific positions. Electron-withdrawing groups, such as fluorine, can increase the lipophilicity of the molecule, potentially enhancing its ability to pass through cell membranes. Conversely, electron-donating groups, like the methyl group, may contribute to the compound's stability. Figure 2, presents the molecular structure of the synthesized compounds, which were subsequently assessed for *in vitro* biological activity.

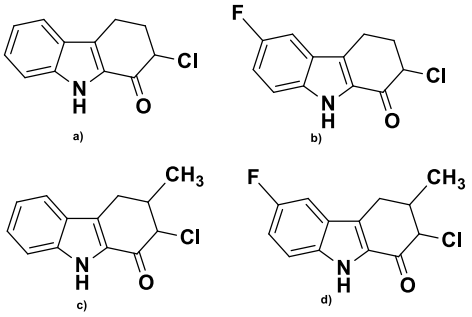

Figure 2. Chemical structure of synthesized compounds a) 9 b) 10 c) 11 d) 12.

The synthetic design showcases strategic use of classical oxidation via periodic acid and Cu(II)-mediated halogenation reactions that are hallmarks of heterocyclic organic synthesis. These transformations illustrate how electron-rich nitrogen heterocycles can be regioselectively functionalized. The mild reaction conditions, good yields, and clean conversions underline the synthetic robustness of this methodology, marking it as valuable for medicinal organic chemistry.

2.2 Molecular docking

The synthesized derivatives demonstrated strong binding affinities compared to the reference compound, INH. Table S1 (in supplimentary file) presents the binding energy, conventional hydrogen bonds, bond lengths, hydrophobic interactions, and other relevant interactions. The reference compound INH showed a binding energy of -5.9, with ASN B:1640 forming a conventional hydrogen bond, and hydrophobic interactions with TYR B:1663, ALA B:1667, TYR B:1674, ASP B:1644, and ILE B:1643 as showed in Figure S25. The derivatives **9, 10, 11,** and **12** exhibited binding energies of -8.0, -8.3, -8.4, and -8.8, respectively. Based on the amino acid interactions detailed in Table S1, the synthesized compounds **9, 10, 11,** and **12** interact at the same site as the standard compound INH. It must be noted that molecular docking alone does not confirm target inhibition. The results provide a hypothetical model of binding and require further validation through biological or biochemical assays.

2.3 Drug likeness and ADMET study

The drug-likeness, ADME (Absorption, Distribution, Metabolism, and Excretion), and toxicity profiles of the molecules were assessed using the PreADMET and SwissADME software (http://www.swissadme.ch/). The parameters and their observed values are summarized in Table S2 in supplementary file. Pharmacokinetic and drug-likeness properties were calculated for each derivative. The derivatives satisfied the Lipinski rule, which includes criteria for the number of hydrogen donors (≤5), hydrogen acceptors (≤10), molecular weight (≤500), and ClogP (≤5), indicating favourable drug-like properties. The data also show that all derivatives exhibit high gastrointestinal absorption, with no violations of the Rule of Five (RFV). The logP values of the derivatives fall between 1 and 4, suggesting ideal lipophilicity. The derivatives **9, 10, 11,** and **12** demonstrated good plasma protein binding (PPB) with values of 100%, 96.60%, 93.28%, and 93.29%, respectively, indicating strong binding to plasma proteins. The Human Intestinal Absorption (HIA%) of the derivatives ranged between 70% and 100%, which indicates excellent absorption potential. Caco-2 cell permeability values for the derivatives ranged from 4 to 70, indicating moderate permeability, as shown in Table S2**.** The toxicity profiles of the designed derivatives are presented in Table S2, covering hepatotoxicity, carcinogenicity, immunotoxicity, mutagenicity, and cytotoxicity.

2.4 Antitubercular activity

The antimycobacterial effectiveness of the derivatives (**9-12**) was evaluated against *Mtb* ATCC 27294 using the MABA at the Department of Microbiology, Maratha Mandal's NGH Institute of Dental Sciences and Research Centre in Belgaum, India. This assay follows a macro dilution protocol and employs a non-toxic, thermally stable reagent that has shown good correlation with other commonly used methods, such as the proportional and BACTEC radiometric methods. For the synthesised compounds, the assay was carried out from 0.8 µg/ml to 100µg/ml. By observing the color change (Figure S26) for both standard drug assay and synthesised compound assay, specifically when the blue color remains unaffected, the concentration at which the derivatives exhibited effective inhibition could be determined. This concentration is referred to as the MIC, which serves to evaluate the effectiveness of the derivatives. For comparison, standard MIC values were established for Pyrazinamide (3.125 µg/ml), Streptomycin (6.25 µg/ml), and Ciprofloxacin (3.125 µg/ml). Table S3 (in supplimentary file) shows the MIC values of the derivatives (**9-12**) alongside the reference drugs, and indicates whether the derivatives are sensitive or resistant at the given concentrations. Based on the data, derivative **12** was found to be the most potent compound when compared to the standard drugs. The observed activity may also be due to general cytotoxicity rather than specific anti-tubercular effects. Further studies are needed to evaluate the selectivity of the compounds using normal or healthy cell lines.

2.5 SAR study of synthesized compounds

Although limited by the small number of derivatives, the SAR of 2-chloro-2,3,4,9-tetrahydro-1H-carbazol-1-one as an antitubercular agent offers some preliminary insights. The tetrahydrocarbazole framework appears crucial for bioactivity, likely through interactions such as π-π stacking or hydrogen bonding with the mycobacterial target. The ketone group at the 1-position may enhance electronic properties and contribute to hydrogen bonding, facilitating target binding. The 2-chloro substitution might increase lipophilicity, potentially aiding in cell wall penetration of Mtb. Modifications at position 2, such as replacing chlorine with other halogens, could influence lipophilicity and steric effects, thereby affecting activity and pharmacokinetics. Additionally, substituents on the aromatic ring, whether electron donating (e.g., -OH, $-OCH_3$) or electron withdrawing (e.g., $-NO_2$, $-CF_3$), might modulate electronic density and binding affinity. The position of these substituents (meta or para) may also play a role in determining the antitubercular activity.

These results provide early insights but are not sufficient to establish definitive SAR. Future research should focus on expanding the structural diversity of tetrahydrocarbazolone derivatives by exploring a broader range of substituents, particularly halogens and electron-donating/withdrawing groups, at strategic positions on the aromatic and saturated rings. Substitution at the 2-position, currently occupied by chlorine, could be varied to enhance physicochemical properties, improve binding affinity to Pks13, and modulate ADMET profiles. Mechanistic studies should be undertaken to elucidate the exact interaction of these compounds with their molecular targets. Furthermore, *in vivo* pharmacokinetics and toxicity profiling, alongside preclinical efficacy testing, are essential next steps. Continued integration of synthetic organic chemistry, SAR analysis, and computational modelling will be pivotal in refining these scaffolds into potent, selective, and safe anti-tubercular agents.

Conclusions

This study highlights the successful design and synthesis of a series of 2-chloro-2,3,4,9-tetrahydro-1*H*-carbazol-1-one derivatives using an efficient three-step organic synthetic route. The application of regioselective

oxidation and electrophilic halogenation underscores the significance of modern heterocyclic chemistry in developing biologically active scaffolds. Structural elucidation using NMR, IR, and HRMS confirmed the integrity of the synthesized compounds. Among these, compound **12** showed superior antitubercular activity, both in vitro and through molecular docking against Pks13. These findings validate the utility of organic synthesis in generating novel pharmacophores with potential therapeutic relevance, particularly for resistant forms of tuberculosis.

Experimental Section

5.1 Synthesis and characterisation

The chemicals used in this study, including phenylhydrazine, 4-fluorophenylhydrazine, cyclohexanone, 4-methylcyclohexanone, and periodic acid, were procured from Sigma-Aldrich. Solvents such as glacial acetic acid, methanol, dimethyl sulfoxide (DMSO), n-hexane, and ethyl acetate were obtained from Millipore Sigma. Thin-layer chromatography (TLC) was performed on silica gel plates (aluminum foil-backed), using a solvent system of n-hexane and ethyl acetate (7:3). TLC spots were visualized under ultraviolet (UV) light. The melting points of the synthesized compounds were determined using open capillaries with a Labronics LT 115 digital apparatus. Fourier-transform infrared (FTIR) spectra were recorded using a Bruker FTIR spectrometer. ^{1}H Nuclear Magnetic Resonance (NMR) spectra were measured with DMSO as a solvent using Bruker AVANCE III 400 MHz instruments at Savitribai Phule Pune University, India. High-resolution mass spectrometry (HRMS) data were obtained using the High IMPACT HD instrument at the same university, with DMSO as the solvent, and analyzed using Chromeleon Xpress software.

General procedure of synthesis: The synthesis of 2-chloro-2,3,4,9-tetrahydro-1H-carbazol-1-one (**9-12**) involves a three-step procedure. In Step 1, substituted tetrahydrocarbazole (**1-4**) was prepared following a previously reported method [20]. Phenylhydrazine and cyclohexanone were refluxed in glacial acetic acid, where the acidic conditions facilitated cyclization to form **1-4** and structure were confirmed by proton NMR which included in the supplementary file as figure S1 to S4. In Step 2, one equivalent of product of step 1 was oxidized to substituted oxo-tetrahydrocarbazole using two equivalents of periodic acid in a methanol-water mixture (1:1). The periodic acid solution, pre-cooled to 0°C, was added dropwise to the solution of **1**, and the mixture was stirred at 0°C for 1 hour, followed by an additional 1-1.5 hours at room temperature. The product **5-8** was isolated by drying and washing with methanol and structure were confirmed by proton NMR which included in the supplementary file as figure S5 to S8. In Step 3, the final product (**12**) was synthesized by dissolving one equivalent of **5-8** in 20 mL of DMSO, followed by the addition of two equivalents of $CuCl_2 \cdot 2H_2O$. The reaction mixture was stirred at 120°C for 15 minutes and then cooled in an ice bath, leading to the precipitation of the final product, which was isolated as **9-12** and structure were confirmed by IR, proton NMR and HRMS spectra which included in the supplementary file as IR data (figure S9 to S12), proton NMR data (figure S13 to S16), Carbon NMR data (figure S17 to S20) and HRMS data (figure S21 to S24).

An optimized synthesis scheme is crucial for preparing the desired derivatives with high practical yields, ensuring repeatability and time efficiency. Scheme 1, illustrates the synthesis pathway for the final 2-chloro-2,3,4,9-tetrahydro-1*H*-carbazol-1-one derivatives.

From the NMR spectra of first (**1-4**) and second intermediates (**5-8**) as mentioned in supplementary file (figure S1-S8), structures of all the intermediates are confirmed. Proton NMR spectral data is found to be matching with the synthesized compound structures and is summarized as follows.

2,3,4,9-tetrahydro-1*H*-carbazole (1). ^{1}H NMR (400 MHz, DMSO): δ 10.634 (s, N-H, 1H), 7.342-7.361 (d, *J* 7.6, aromatic C-H, 1H), 7.254-7.273 (d, *c*7.6, aromatic C-H, 1H), 6.939-7.007 (m, aromatic C-H, 2H), 2.645-2.727 (m, cyclic CH_2, 4H), 1.857 (s, cyclic CH_2, 4H).

6-fluoro-2,3,4,9-tetrahydro-1*H*-carbazole (2). ^{1}H NMR (400 MHz, DMSO): δ 10.784 (s, N-H, 1H), 7.232-7.265 (dd, *J* 4.4, 4, 4.8, aromatic C-H, 1H), 7.082-7.112 (dd, *J*.2.4, 7.6, 2, aromatic C-H, 1H), 6.808-6.860 (t, aromatic C-H, 1H), 2.548-2.732 (m, cyclic CH_2, 4H), 1.833-1.883 (m, cyclic CH_2, 4H).

3-methyl-2,3,4,9-tetrahydro-1*H*-carbazole (3). ^{1}H NMR (400 MHz, DMSO): δ 10.672 (s, N-H, 1H), 7.356-7.375 (d, *J* 7.6, aromatic C-H, 1H), 7.274-7.293 (d, *J*.7.6, aromatic C-H, 1H), 6.959-7.026 (m, aromatic C-H, 2H), 2.785-2.835 (m, cyclic CH_2, 2H), 2.211-2.272 (m, cyclic CH_2, cyclic CH, 3H), 1.941-1.968 (d, *J*.10.8, cyclic CH, 1H),1.142-1.158 (d, *J* 6.4, CH_3, 3H).

6-fluoro-3-methyl-2,3,4,9-tetrahydro-1*H*-carbazole (4). ^{1}H NMR (400 MHz, DMSO): δ 10.804 (s, N-H, 1H), 7.241-7.274 (dd, *J* 4.8, 4, 4.4, aromatic C-H, 1H), 7.087-7.111 (d, J 9.6, aromatic C-H, 1H), 6.842 (s, aromatic C-H, 1H), 2.759- 2.782 (m, cyclic CH_2, 2H), 2.173-2.210 (m, cyclic CH, 1H) 1.930 (s, cyclic CH_2, 2H), 1.522-1.543 (d, *J* 8.4, cyclic CH, 1H), 1.131-1.147 (d, J 6.4, CH_3, 3H).

2,3,4,9-tetrahydro-1*H*-carbazol-1-one (5). ^{1}H NMR (400 MHz, DMSO): δ 11.794 (s, N-H, 1H), 8.094 (s, aromatic C-H, 1H), 7.557-7.699 (m, aromatic C-H, 1H), 7.265-7.435 (m, aromatic C-H, 1H), 7.085-7.122 (m, aromatic C-H, 1H), 2.959-2.975 (d, *J* 6.4, cyclic CH_2, 2H), 2.532-2.601 (m, cyclic CH_2, 2H), 2.163-2.178 (d, J 6, cyclic CH_2, 2H).

6-fluoro-2,3,4,9-tetrahydro-1*H*-carbazol-1-one (6): ^{1}H NMR (400 MHz, DMSO): δ 11.711 (s, N-H, 1H), 7.412-7.499 (m, aromatic C-H, 2H), 7.198-7.227 (t, aromatic C-H, 1H), 2.933-2.962 (dd, J 5.6, 6, cyclic CH_2, 2H), 2.577-2.609 (t, *J* 6.4, cyclic CH_2, 2H), 2.175-2.190 (d, J 6, cyclic CH_2, 2H).

3-methyl-2,3,4,9-tetrahydro-1*H*-carbazol-1-one (7). ^{1}H NMR (400 MHz, DMSO): δ 11.608 (s, N-H, 1H), 7.674-7.694 (d, J=8, aromatic C-H, 1H), 7.328-7.437 (m, aromatic C-H, 2H), 7.085-7.122 (dd, J 7.6, 7.2, aromatic C-H, 1H), 3.096-3.144 (d, *J*.16, cyclic CH, 1H), 2.409-2.565 (m, cyclic CH_2, cyclic CH, 3H), 1.182 (s, CH_3, 3H).

6-fluoro-3-methyl-2,3,4,9-tetrahydro-1*H*-carbazol-1-one (8). ^{1}H NMR (400 MHz, DMSO): δ 11.708 (s, N-H, 1H), 7.406-7.469 (m, aromatic C-H, 2H), 7.163- 7.214 (m, aromatic C-H, 1H), 3.055-3.095 (d, J=16, cyclic CH, 1H), 2.398-2.558 (m, cyclic CH_2, cyclic CH, 3H), 1.162 (s, CH_3, 3H).

The physical properties of the synthesized derivatives (**9-12**) are summarized below which includes a molecular formula., Molecular weight, melting point, Percentage yield, and R_f value and the spectroscopy results included FTIR, ^{1}H NMR, and HRMS of the compounds. All the spectral data is found to be matching with the synthesized compound structures and is summarized as follows.

2-chloro-2,3,4,9-tetrahydro-1*H*-carbazol-1-one (9). Appearance: Brown solid; Yield: 75%; R_f: 0.35; MP: 160-162°C; FT-IR: 3278 (N-H), 2915 (C-H), 1651 (C=O), 706 (C-Cl); ^{1}H NMR (400 MHz, DMSO): δ 11.814 (s, N-H, 1H), 8.131 (s, aromatic C-H, 1H), 7.590-7.722 (d, *J*.8, 8.4, aromatic C-H, 1H), 7.263-7.586 (m, aromatic C-H, 1H), 7.103 (s, aromatic C-H, `1H), 4.979 (s, cyclic C-H, 1H), 3.085 (s, cyclic CH_2, 2H), 2.639-2.672 (m, cyclic CH_2, 2H); ^{13}C NMR (101MHz, DMSO): 18.84, 34.42, 84.20, 113.36, 115.73, 120.57, 125.34, 127.45, 129.87, 135.20, 139.32; 183.66; HRMS (ESI) *m/z*: [M+H]+ calcd for $C_{12}H_{10}ClNO$, 219.0451; found 220.0524

2-chloro-6-fluoro-2,3,4,9-tetrahydro-1*H*-carbazol-1-one (10). Appearance: Brown solid; Yield: 72%, R_f: 0.32; MP: 139-141°C; FT-IR: 3274 (N-H), 2936 (C-H), 1647 (C=O), 1442 (C-H bending), 1217 (C-N), 812 (C-Cl), 732 (C-F); ^{1}H NMR (400 MHz, DMSO): δ 11.931 (s, N-H, 1H), 7.505-7.534 (d, J=8, aromatic C-H, 1H), 7.415-7.449 (dd, *J*.4.4, 9.2, aromatic C-H, 1H), 7.263-7.436 (d, *J*.2.4, aromatic C-H, 1H), 4.971-4.999 (dd, *J*.4,7.2 cyclic CH, 1H), 3.054-3.065 (m, cyclic CH_2, 2H), 2.637-2.682 (dd, *J*.5.2, 4.8, 4, cyclic CH_2, 2H); ^{13}C NMR (101MHz, DMSO): 18.84, 34.31, 61.18, 106.21, 114.75, 116.54, 116.28, 128.23, 130.85, 136.00, 156.37, 183.86; HRMS (ESI) *m/z*: [M+H]+ calcd for $C_{12}H_9ClFNO$, 237.0357; found 238.0430

2-chloro-3-methyl-2,3,4,9-tetrahydro-1*H*-carbazol-1-one (11). Appearance: Brown solid; Yield: 70%; R_f: 0.39; MP: 133-135°C; FT-IR: 3282 (N-H), 2924 (C-H), 2828 (C-H alkane), 1647 (C=O), 1254 (C-N), 790 (C-Cl); ^{1}H NMR (400 MHz, DMSO): δ 11.803 (s, N-H, 1H), 7.719-7.699 (d, J.8, aromatic C-H, 1H), 7.433-7.338 (m, aromatic C-H, 2H), 7.101-7.138 (dd, *J*.7.2, 7.6, aromatic C-H, 1H), 4.633-4.885 (d, *J* 9.2, cyclic CH, 1H), 3.047-3.087 (d, *J*.16, cyclic CH, 1H), 2.753-2.807 (m, cyclic CH_2, 2H), 1.223-1.296 (m, CH_3, 3H); ^{13}C NMR (101MHz, DMSO): 19.80, 25.32, 37.13, 66.73, 113.36, 120.59, 121.87, 125.28, 127.16, 128.36, 129.46, 139.42, 183.75; HRMS (ESI) *m/z*: [M+H]+ calcd for $C_{13}H_{12}ClNO$, 233.0607; found 234.0686

2-chloro-6-fluoro-3-methyl-2,3,4,9-tetrahydro-1*H*-carbazol-1-one (12). Appearance: Brown solid; Yield: 72%; R_f: 0.31; MP: 146-148°C; FT-IR: 3280 (N-H), 2923 (C-H), 1650 (C=O), 1253 (C-N), 790 (C=Cl), 703 (C-F). ^{1}H NMR (400 MHz, DMSO) δ 11.940 (s, N-H, 1H), 7.414-7.516 (m, aromatic C-H, 2H), 7.208-7.254 (m, aromatic C-H, 1H), 4.673 (s, cyclic CH, 1H), 3.008-3.058 (m, cyclic CH, 1H); 2.679-2.811 (m, cyclic CH_2, 2H), 1.226 (m, CH_3, 3H). ^{13}C NMR (101MHz, DMSO): 17.74, 27.84, 32.86, 66.53, 105.60, 114.52, 116.26, 125.15, 127.52, 130.23, 135.27, 158.67, 183.83; HRMS (ESI) *m/z*: [M+H]+ calcd for $C_{13}H_{11}ClFNO$, 251.0513; found 252.0593.

5.2 Computational details of molecular docking

5.2.1 Selection and Preparation of Protein:

Proteins were visualized and examined from dataset of RCSB Protein data bank (PDB) (https://www.rcsb.org/) website. The selection of the protein was based on the structure should be established by X ray diffraction and its resolution should be between 1.5 to 3.0 Å which is ideal to form a bond with ligand. 5V3Y codes for Crystal Structure of Mtb Pks13 Thioesterase domain in complex with inhibitor TAM16 (5V3Y protein DOI-https://doi.org/10.2210/pdb5V3Y/pdb) having resolution 1.98Å. The protein was prepared by using Biovia Discovery Studio (v21.1.0) in such a way that there is a removal of all heteroatoms and water molecules, ions etc. and crystal structure of protein was further saved as prepared protein structure [21].

5.2.2 Ligand Preparation:

Tetrahydrocarbazole derivatives were designed using ChemDraw Ultra 12.0, converted to 3D models in Chem3D Pro 12.0, and saved in PDB format. The structure data file (SDF) for INH was downloaded from PubChem (https://pubchem.ncbi.nlm.nih.gov).

5.2.3 Molecular docking:

PyRx 0.8 (https://pyrx.sourceforge.io/; https://sourceforge.net/projects/pyrx/) was used to carry out molecular docking. This tool is easy to use and it integrated by Autodock, vine wizard and open babel. This software mostly coordinates with the SDF file or PDB file to carry out docking. Firstly, load the prepared protein in software and then convert it to PDBQT format by clicking on “make macromolecule “and check this format in Autodock. After that add all ligands in open babel and minimize energies of all the ligands and convert it to PDBQT format [17]. The grid box parameter file was generated by adjusting dimensions axis x, y, z from 25×25×25 to 68.18×82.57×72.27 respectively and cell origin was x, y, z from 11.29×30.85×16.12 to 13.94×45.63×5.51 respectively. After the preparation start docking using Vina wizard which will give the docking score of various conformations of protein-ligand interaction from which the ligand which have highest docking score will have best affinity. Molecular interaction of protein and ligand was investigated by using BIOVIA discovery studio 2021.[22]

5.3 Drug likeness and ADMET study

The PreADMET software (https://preadmet.webservice.bmdrc.org/) was used to estimate the compounds' drug-likeness, ADME, and toxicity profiles. Physicochemical characteristics including water solubility, polar surface area, molecular weight, and lipophilicity (logP) are intimately associated with ADME/Tox features. The software produced data demonstrating drug-likeness (e.g., CRV - CMC rule violation, MDDRRV, RFV - Rule of Five violation) and hydrogen bond donor (HBD) and acceptor (HBA) features after the suggested derivative

structures were created. The derivatives' ADME characteristics included Caco-2 permeability, HIA (Human Intestinal Absorption), BBB (Blood-Brain Barrier penetration), percentage PPB (Plasma Protein Binding), and toxicity tests (e.g., carcinogenicity in mice or rats, Ames test, etc.). The CMC rule's qualifying ranges include logP between -0.4 and 5.6, molecular weight between 160 and 480, molar refractivity between 40 and 130, and the total number of atoms between 20 and 70. CRV is comparable to RFV. The following conditions determine RFV: CLogP ≤ 5 (MlogP ≤ 4.5), MW ≤ 500, HBD ≤ 5, and HBA ≤ 10. According to the MDDR-like rule, a chemical has a high likelihood of being "drug-like" if the following criteria are satisfied: Number of Rotatable Bonds > 6, Number of Rings ≥ 3, and Number of Rigid Bonds ≥ 18. A molecule is more likely to be "non-drug-like" if, on the other hand: No. of Rotatable Bonds < 5, No. of Rings ≤ 2, and No. of Rigid Bonds ≤ 17. When combined, these three factors characterize the drug-likeness of the compound. From the PreADMET software, the following parameters were evaluated: HIA, BBB penetration, PPB model, Caco-2 cell permeability, mutagenicity, and carcinogenicity.

5.4 In vitro antitubercular activity using MABA assay

Microplate Alamar Blue Dye Assay: This method is widely used for evaluating of derivatives. The anti-mycobacterial activities of the synthesized derivatives were assessed against Mtb (H37 RV strain): ATCC NO.: 2729 by using MABA. The method is non-toxic uses a thermally stable reagent, and demonstrates good correlation with proportional and BACTEC radiometric methods. The Alamar Blue Reagent is important for assay and is added in wells containing culture. It is added to each well of the microplate that contains Mtb culture and varying concentrations of the antitubercular compound. In order to validate the assay, appropriate controls are included. A well with no drug serves as the negative control to assess the normal growth of Mtb, while a well with a known antitubercular drug, such as rifampicin, acts as the positive control to ensure the assay is functioning correctly. The microplate is systematically arranged with rows assigned to different concentrations of the antitubercular compound. For each concentration, three duplicate wells are used to ensure duplicates for statistical significance. Separate wells are allocated for the negative and positive controls. After the setup, the microplate is incubated at 37°C in a humidified atmosphere, or at any other temperature that is adequate for Mtb growth. This promotes the development of germs over a predetermined incubation period, typically 5-7 days. Using a spectrophotometer or a microplate reader, the colour change in each well is detected when the incubation period is over. This readout allows the assessment of bacterial growth inhibition or viability. Every well's absorbance or fluorescence is measured, and the data is then examined. By analysing the extent of colour change, one can determine the effectiveness of the compound in inhibiting bacterial growth. To ensure reliable and statistically significant results, the assay is performed in triplicate for each concentration of the antitubercular compound. This provides replicates for robust data analysis. The MIC is then calculated by identifying the lowest concentration of the compound that produces a noticeable change in colour compared to the negative control wells. This concentration indicates a significant reduction in bacterial growth or viability. Finally, the tested compound's activity is compared with that of known antitubercular agents to assess its efficacy. This comparison involves comparing the MIC values of the tested compound with those of established antitubercular drugs such as isoniazid or ethambutol. Such comparative analysis offers insights into the relative potency and effectiveness of the compound being tested in the context of existing treatments for tuberculosis. Basic procedure was, 200µl of sterile deionized water was added to all outer perimeter wells of the sterile 96-well plate to minimize evaporation of medium in the test wells during incubation. A 96-well plate was filled with 100 µl of Middlebrook 7H9 broth, and serial dilutions of the compounds were prepared directly within the plate. The final drug concentrations ranged from 100 to 0.2 µg/ml. The plates were then covered, sealed with parafilm, and incubated at 37°C for five days. Following incubation, 25 µl of a freshly prepared 1:1 mixture of Alamar Blue reagent and 10% Tween 80 was added to each well, and the plates were incubated for an additional 24 hours.

A blue color in the wells indicated no bacterial growth, while a pink color signified bacterial growth. The MIC was determined as the lowest drug concentration that inhibited the color change from blue to pink [23–25].

Acknowledgements

Authors thankful to the Dr. Vishwanath Karad MIT-World Peace University, Pune for supporting to carry out research work. Authors also thankful to the department of Microbiology, Maratha Mandal's NGH Institute of Dental Sciences and Research Centre in Belgaum, India for providing facilities to carry out *in vitro* study for antituberculosis.

Supplementary Material

The data that supports the findings of this study are available in the supplementary material of this article. NMR spectra of 1-4 and 5-8 as mentioned in supplementary file from figure S1-S4 and figure S5-S8 respectively. FTIR, 1H NMR, and HRMS of the compounds (9-12) are included in supplementary file from Figure S9-S20.

Author contribution

The contributions of all the authors to a manuscript must be described in the following format: ARC has designed the research; PSW and SSB have performed the experiments; ARC and PSM have analyzed the data; PSW and SSB have wrote the manuscript draft; PSM revised the manuscript. All authors approved the final version of the manuscript.

Conflict of interest

Author declares no potential conflict of interest.

References

1. Mandal, S.; Rao, R.; Joshi, R. *Indian J. Community Med.* **2023**, *48*, 436–442. https://doi.org/10.4103/ijcm.ijcm_160_23.
2. Dartois, V. A.; Rubin, E. J. *Nat. Rev. Microbiol.*, **2022**, 685–701. https://doi.org/10.1038/s41579-022-00731-y.
3. Zumla, A. I.; Gillespie, S. H.; Hoelscher, M.; Philips, P. P. J.; Cole, S. T.; Abubakar, I.; McHugh, T. D.; Schito, M.; Maeurer, M.; Nunn, A. J. *Lancet Infect. Dis*. **2014**, 327–340. https://doi.org/10.1016/S1473-3099(13)70328-1.
4. Chauhan, A.; Kumar, M.; Kumar, A.; Kanchan, K. *Life Sci*., **2021**. https://doi.org/10.1016/j.lfs.2021.119301.

5. Ullah, I.; Shah, A. A.; Basit, A.; Ali, M.; khan, A.; Ullah, U.; Ihtesham, M.; Mehreen, S.; Mughal, A.; Javaid, A. *BMC Infect. Dis.* **2016**, *16*. https://doi.org/10.1186/s12879-016-1745-2.
6. Wang, G.; Sun, S.; Guo, H. *Eur. J. Med. Chem.* **2022**, *229*, 113999. https://doi.org/10.1016/J.EJMECH.2021.113999.
7. Su, L.; Li, J.; Zhou, Z.; Huang, D.; Zhang, Y.; Pei, H.; Guo, W.; Wu, H.; Wang, X.; Liu, M.; Yang, C. G.; Chen, Y. *Eur. J. Med. Chem.* **2019**, *162*, 203–211. https://doi.org/10.1016/j.ejmech.2018.11.016.
8. Puglsey T. A.; Lippmann W. *Experientia* **1977**, 33, 57-9. doi: 10.1007/BF01936753.
9. Scatina, J. A.; Hicks, D. R.; Kraml, M.; Cayen, M. N. *Xenobiotica* **1989**, *19*, 991–1002. https://doi.org/10.3109/00498258909043156.
10. Caruso, A.; Ceramella, J.; Iacopetta, D.; Saturnino, C.; Mauro, M. V.; Bruno, R.; Aquaro, S.; Sinicropi, M. S. *Molecules*, **2019**. https://doi.org/10.3390/molecules24101912.
11. Gudmundsson, K. S.; Sebahar, P. R.; Richardson, L. D. A.; Catalano, J. G.; Boggs, S. D.; Spaltenstein, A.; Sethna, P. B.; Brown, K. W.; Harvey, R.; Romines, K. R. *Bioorg. Med. Chem. Lett.* **2009**, *19*, 3489–3492. https://doi.org/10.1016/j.bmcl.2009.05.003.
12. Sibaji Sarkar; Shubham Makvana; Disha Hirani; Isha Makadia; Khyati Dholariya; Harsh Dhokia; Nency Vanpariya. *World J. Adv. Res. Rev.* **2023**, *21*, 2127–2135. https://doi.org/10.30574/wjarr.2024.21.3.0935.
13. Bailo, R.; Radhakrishnan, A.; Singh, A.; Nakaya, M.; Fujiwara, N.; Bhatt, A. *Sci. Rep.* **2022**, *12*, 6943. https://doi.org/10.1038/s41598-022-10589-y.
14. Xia, F.; Zhang, H.; Yang, H.; Zheng, M.; Min, W.; Sun, C.; Yuan, K.; Yang, P. *Eur. J. Med. Chem*., **2023**. https://doi.org/10.1016/j.ejmech.2023.115702.
15. Portevin, D.; De Sousa-D'Auria, C. L.; Houssin, C.; Grimaldi, C.; Chami, M.; Daffé, M.; Guilhot, C. Proc. *Natl. Acad. Sci*. U.S.A. **2004**, 101, 314. www.pnas.orgcgidoi10.1073pnas.0305439101.
16. Ejalonibu, M. A.; Ogundare, S. A.; Elrashedy, A. A.; Ejalonibu, M. A.; Lawal, M. M.; Mhlongo, N. N.; Kumalo, H. M. *Int. J. Mol. Sci*., **2021**. https://doi.org/10.3390/ijms222413259.
17. Aggarwal, A.; Parai, M. K.; Shetty, N.; Wallis, D.; Woolhiser, L.; Hastings, C.; Dutta, N. K.; Galaviz, S.; Dhakal, R. C.; Shrestha, R.; Wakabayashi, S.; Walpole, C.; Matthews, D.; Floyd, D.; Scullion, P.; Riley, J.; Epemolu, O.; Norval, S.; Snavely, T.; Robertson, G. T.; Rubin, E. J.; Ioerger, T. R.; Sirgel, F. A.; van der Merwe, R.; van Helden, P. D.; Keller, P.; Böttger, E. C.; Karakousis, P. C.; Lenaerts, A. J.; Sacchettini, J. C. *Cell* **2017**, *170*, 249-259.e25. https://doi.org/10.1016/j.cell.2017.06.025.
18. Abdullahi, M.; Adeniji, S. E. *Chem. Afr.* **2020**, *3*, 989–1000. https://doi.org/10.1007/s42250-020-00162-3.
19. Bielenica, A.; Głogowska, A.; Augustynowicz- Kopeć, E.; Orzelska-Górka, J.; Kurpios-Piec, D.; Struga, M. *Tuberculosis* **2023**, *143*. https://doi.org/10.1016/j.tube.2023.102412.
20. Nitin Kumar; Vinod Kumar; Yogita Chowdhary. *World J. Adv. Res. Rev.* **2022**, *13*, 160–171. https://doi.org/10.30574/wjarr.2022.13.1.0754.
21. Piton, J.; Vocat, A.; Lupien, A.; Foo, C. S.; Riabov, O.; Makarov, V.; Cole, S. T. *Antimicrob. Agents Chemother.* **2018**, *62*. https://doi.org/10.1128/AAC.00681-18.

22. Parween, A. *Int. J. Res. Appl. Sci. Eng. Technol.* **2020**, *8*, 2421–2427. https://doi.org/10.22214/ijraset.2020.6389.
23. Vadivel, E.; Arondekar, S. G. *Int. Res. J. Pharm. Med. Sci.* **2018**, *1*, 46–48.
24. Kumar, V.; Shetty, P.; Arunodaya, H. S.; Chandra K., S.; Ramu, R.; Patil, S. M.; Baliga, A.; Rai, V. M.; Shalini Shenoy, M.; Udupi, V.; Poojary, V.; Poojary, B. *Chem. Biodivers.* **2022**, *19*. https://doi.org/10.1002/cbdv.202100532.
25. Posinasetty, B.; Yejjella, R. P.; Birudala, G.; Bandarapalle, K.; Rajasekhar, K. K.; Chilamakuru, N. B. *Asian J. Chem.* **2023**, *35*, 2979–2986. https://doi.org/10.14233/ajchem.2023.30319.